An Aligned Magnetic Field Effect on Unsteady Heat and Mass Transfer Flow of Non-Newtonian Fluid Through Porous Medium

S. Rama Mohan (ID)**, N. Maheshbabu** (ID)**, and M. Eswara Rao** (ID)

1 Introduction

When a force is applied to non-Newtonian fluids, the viscosity may change, becoming more liquid or perhaps more solid. Fluid viscosity depends linearly on shear stress. Examples of non-Newtonian fluids are blood, honey, ketchup, toothpaste, peanut oil, paints, and inks. The typical viscous fluid model is unable to explain the ductile fracture characteristic of non-Newtonian fluids; however, Jeffrey's liquid model can. The fluid model proposed by Jeffrey is a useful tool for describing the class of non-Newtonian fluids with their distinctive recollection time scales, also referred to as relaxation time. Several authors contributed their analysis of non-Newtonian fluids with the assistance of mathematical modeling. Rundora et al. [1] studied non-Newtonian fluid unstable MHD reactive flow over a porous filled medium with irregular circumferential layer examples. Eddy et al. [2] have discussed the effects of an aligned magnetic field on the Casson liquid flow via a vertical oscillation plate in a porous medium. Jena et al. [3] described that a chemical reaction has an impact on the flow of Jeffery MHD fluid on a stretched surface via a porous medium. An associated irresistible field has an impact on the unstable fluid flow of Casson liquid over a stretch sheet examined by Sailaja et al. [4]. Non-

S. Rama Mohan
Department of Mathematics, PACE Institute of Technology & Sciences (Autonomous), Ongole, A.P, India

N. Maheshbabu (✉)
Department of Mathematics, Dr.S.R.K. Govt Arts College, Yanam, U.T. of Puducherry, India
e-mail: nmahesh@dhtepdy.edu.in

M. Eswara Rao
Department of Mathematics, Saveetha School of Engineering, SIMATS, Chennai, Tamil Nadu, India

Newtonian Ferro fluid flow across an unsteady contracted cylinder underneath the effect of an associated irresistible field was studied by Saranya et al. [5]. Santoshi et al. [6] scrutinized non-Newtonian liquid flow characteristics through a parabolic reflector of rotation and discussed them. Thermal effects and an inclined irresistible field on the MHD free convection flow of Casson fluid through a segmentation were investigated by Kumar et al. [7]. An unstable MHD dual diffusional free convection movement of Kuvshinski fluid is affected by an irresistible field across an inclined, movable porosity surface. This has been studied by Rama Prasad et al. [8]. Endalew et al. [9] defined a porous medium as the location of the occurrences of the irresistible field oriented on an unsteady MHD that passes in front of an inclined plate with parabolic acceleration. Abd-Alla et al. [10], in the presence of heat and mass transfer, investigated the impact of an inclined magnetism on the peristaltic blood flow in an asymmetrical porous channel. Kodi et al. [11] studied heat and mass transfer using a vertical inclination porosity surface with Soret thermal diffusion, an associated magnetic field, and the magnetohydrodynamic convective unsteady flow of a Jeffrey fluid. In their study, Nazir et al. [12]. On the heat and mass transmission of non-Newtonian liquids involving interface chemical processes. The analysis of heat and mass transmission above an unstable infinite porous material with a chemical process was discovered by Arshad et al. [13].

The influence of viscous dissipation and buoyancy force on the Jeffrey fluid's inconsistent flow in a vertical porous layer with changing viscosity has not, as far as we are aware, been investigated. To comprehend the alignment of irresistible field influence on the unsteady heat and mass transfer flow of non-Newtonian Jeffrey fluid through porous media under the influence of chemical response and heat absorption, the current problem is modeled. The geological processes in the Earth's mantle, MHD compressors, accelerators, geothermal reservoirs, and subsurface energy transport are all important applications for this model. The chapter is also structured as follows. The plate's lengthwise periodic oscillation induces the flow, and a uniform transversal irresistible field is supplied in the direction of the flow.

Using the Laplace transform approach, the systems of non-dimensional dominating PDEs are analytically solved. Graphs and tables are used to derive and discuss the effects of various flow quantities on velocity, temperature, and concentration, in addition to the frictional pressure coefficient and the rate of mass and heat transfer factors.

2   Mathematical Formulation

The fluid flow is transversely subjected to a uniform magnetic field B while an unstable MHD convective heat and mass transfer of a viscous, immiscible, electrically conducting, radiative, and chemically reactive fluid passes past a vertical plate. Assume that the x*-axis is taken perpendicular to the surface and that the y*-axis is parallel to the surface in the direction of the transversal magnetic field that is being provided. The fluid and the surface were originally static, with constant

temperatures and concentrations at the time $t* \leq 0$. The plate starts oscillating on its surface with a velocity of $z = Z_o \cos(w*t*)$ against the gravity field whenever $t* > 0$, where w* denotes the magnitude of the surface oscillation. The tube's concentration and heating are increased to θ_w^* and $\varnothing_w^*$ both at the same time. It is considered that a consistent magnetic field B_0 is applied normally to the flow. So, because the high Reynolds numbers of the flux are thought to be very low, it is also expected that the irresistible field it induces will be minimal for free convection flow. The fluid that is being thought about here is gray, which absorbs/emits radiation, but it is not a dispersion medium. The mathematical model (see References [8, 9]) is listed below.

Momentum Equation:

$$\frac{\partial z*}{\partial t*} = v \left(\frac{1}{1+\lambda}\right) \frac{\partial^2 z*}{\partial y*^2} - \frac{\sigma B_0^2 \sin^2\alpha}{\rho} z* - \frac{v}{K} z* \tag{1}$$

Energy Equation:

$$\frac{\partial \theta*}{\partial t*} = \frac{\kappa}{\rho C_p} \frac{\partial^2 \theta*}{\partial y*^2} - \frac{1}{\rho C_p} \frac{\partial q_r}{\partial y*} - \frac{Q*}{\rho C_p} \left(\theta* - \theta_\infty^*\right) \tag{2}$$

Diffusion Equation:

$$\frac{\partial \phi*}{\partial t*} = D_m \frac{\partial^2 \phi*}{\partial y*^2} - Kr \left(\phi* - \phi_\infty^*\right) \tag{3}$$

According to the original boundary conditions:

$$
\begin{aligned}
&t* \leq 0, z* = 0, \theta* = \theta_\infty^*, \phi* = \phi_\infty^* \; for \; all \; y*, \\
&t* > 0, z* = Z_0 \cos(wt), \quad \theta* = \theta_w^*, \quad \phi* = \phi_w^* \; at \; y* = o, \\
&z* \to 0, \quad \theta* \to \theta_\infty^*, \quad \phi* \to \phi_\infty^* \; as \; y* \to \infty.
\end{aligned}
\tag{4}
$$

Here $z*, \lambda, B_0, v, q_r, Q, \sigma, D_m, t, K, \rho, \theta*, \varnothing*, C_p, C_s, K_T, w, and \; K_r$ are the velocity of the liquid in the x^*- direction, Jeffrey liquid quantity, external magnetic field, kinematic viscosity, concentration susceptibility, radiative heating absorption, the temperature of the liquid near the surface, heat fluctuation, stereotyped potential, coefficient of mass diffusivity, time, thermal potential, liquid capacity species concentration, specific heat at perpetual pressure, periodicity parameter, and chemical reaction quantity, respectively.

Under the Rosseland estimate, the radiant heat variation of the type shown below is used.

$$q_r = -\frac{4\sigma*}{3k*} \frac{\partial \theta*}{\partial y*} \tag{5}$$

Here, $\sigma *$ denotes the Stefan–Boltzmann constant, and $k*$ represents the average absorption ratio. The stream's temperature variation θ^{*^4} is thought to be sufficiently minimal to be stated to be a linear function of temperature. The higher-order terms are disregarded to achieve this and expanding θ^{*^4} a Taylor series about θ^*_∞.

As a result, we get

$$\theta^{*^4} = 4\theta^{*^3}_\infty \theta^* - 3\theta^{*^4}_\infty. \tag{6}$$

Equation (2) reduces after incorporating Eqs. (5) and (6).

$$\frac{\partial \theta^*}{\partial t^*} = \frac{\kappa}{\rho C_P} \frac{\partial^2 \theta^*}{\partial y^{*2}} - \frac{16\sigma^* \theta^*_\infty}{3\rho C_P k^*} \frac{\partial^2 \theta^*}{\partial y^{*2}} - \frac{Q^*}{\rho C_p} \left(\theta^* - \theta^*_\infty \right) \tag{7}$$

Adding the aforementioned dimensionless amounts

$$z = \frac{z^*}{Z_0}, y = \frac{Z_0}{v} y^*, t = \frac{Z_0^2}{v} t^*, M = \frac{\sigma B_0^2 v}{\rho Z_0^2}, \theta = \frac{(\theta^* - \theta^*_\infty)}{(\theta^*_W - \theta^*_\infty)}, K = \frac{k^* z_0^2}{v}, \phi = \frac{(\phi^* - \phi^*_\infty)}{(\phi^*_W - \phi^*_\infty)},$$

$$\mathrm{Pr} = \frac{\rho v C_P}{\kappa}, Q = \frac{Q^* v}{\rho C_p Z_0^2}, R = \frac{16\sigma^* \theta^{*^3}_\infty}{3k^* k} w = w^* \frac{v}{Z_0^2}. \tag{8}$$

Because of Eqs. (1), (3), and (7), transmission constitutes (8)

$$\frac{\partial z}{\partial t} = \left(\frac{1}{1+\lambda} \right) \frac{\partial^2 z}{\partial y^2} - \left(M\sin^2\alpha + \frac{1}{K} \right) z \tag{9}$$

$$\frac{\partial \theta}{\partial t} = \left(\frac{1+R}{\mathrm{Pr}} \right) \frac{\partial^2 \theta}{\partial y^2} - Q\,\theta \tag{10}$$

$$\frac{\partial \phi}{\partial t} = -Kr\,\phi + \frac{1}{Sc} \frac{\partial^2 \phi}{\partial y^2} \tag{11}$$

The associated boundary conditions become

$$\begin{aligned} &z = 0,\ \theta = 0,\ \phi = 0 \ for\ all\ y, t \leq 0, \\ &z = \cos(wt),\ \theta = 1, \phi = 1\ at\ y = 0, t > 0, \\ &z \to 0,\ \theta \to 0,\ \phi \to 0\ as\ y \to \infty, t > 0. \end{aligned} \tag{12}$$

3 Solution of the Problem

By employing the Laplace transform method and the boundary condition formulas (12), the equation system (9) to (11) is parameter estimation.

$$z(y,t) = \frac{e^{iwt}}{4}\left[\begin{array}{l}\exp\left(-y\sqrt{H_3(H_4+iw)}\right)\,\mathrm{erfc}\left(\frac{y\sqrt{H_3}}{2\sqrt{t}}-\sqrt{(H_4+iw)\,t}\right)\\ +\exp\left(y\sqrt{H_3(H_4+iw)}\right)\,\mathrm{erfc}\left(\frac{y\sqrt{H_3}}{2\sqrt{t}}+\sqrt{(H_4+iw)\,t}\right)\end{array}\right]$$
$$+\frac{e^{-iwt}}{4}\left[\begin{array}{l}\exp\left(-y\sqrt{H_3(H_4-iw)}\right)\,\mathrm{erfc}\left(\frac{y\sqrt{H_3}}{2\sqrt{t}}-\sqrt{(H_4-iw)\,t}\right)\\ +\exp\left(y\sqrt{H_3(H_4-iw)}\right)\,\mathrm{erfc}\left(\frac{y\sqrt{H_3}}{2\sqrt{t}}+\sqrt{(H_4-iw)\,t}\right)\end{array}\right]$$

$$\tag{13}$$

$$\theta(y,t) = \frac{1}{2}\left[\begin{array}{l}\exp\left(-y\sqrt{H_1 Q}\right)\,\mathrm{erfc}\left(\frac{y\sqrt{H_1}}{2\sqrt{t}}-\sqrt{Q t}\right)\\ +\exp\left(y\sqrt{H_1 Q}\right)\,\mathrm{erfc}\left(\frac{y\sqrt{H_1}}{2\sqrt{t}}+\sqrt{Q t}\right)\end{array}\right] \tag{14}$$

$$\phi(y,t) = \frac{1}{2}\left[\begin{array}{l}\exp\left(-y\sqrt{Sc\,kr}\right)\,\mathrm{erfc}\left(\frac{y\sqrt{Sc}}{2\sqrt{t}}-\sqrt{Kr t}\right)\\ +\exp\left(y\sqrt{Sc\,Kr}\right)\,\mathrm{erfc}\left(\frac{y\sqrt{Sc}}{2\sqrt{t}}+\sqrt{Kr\,t}\right)\end{array}\right] \tag{15}$$

3.1 Skin-Friction Coefficient

The formula for the skin-graft coefficient at y = 0 is

$$\tau = -\left(\frac{1}{1+\lambda}\right)\left[\frac{\partial z}{\partial y}\right]_{y=0} \tag{16}$$

We derive the following skin-graft coefficient from Eqs. (13) and (16):

$$\tau = \left(\frac{1}{1+\lambda}\right)\left[\begin{array}{l}\frac{e^{iwt}}{2}\left(\sqrt{H_3(H_4+iw)}\mathrm{erf}\left(\sqrt{(H_4+iw)\,t}\right)+\sqrt{\frac{H_3}{\pi t}}e^{-(H_4+iw)t}\right)\\ +\frac{e^{-iwt}}{2}\left(\sqrt{H_3(H_4-iw)}\mathrm{erf}\left(\sqrt{(H_4-iw)\,t}\right)+\sqrt{\frac{H_3}{\pi t}}e^{-(H_4-iw)t}\right)\end{array}\right]$$

3.2 Nusselt Number

Nusselt number at y = 0 is given by

$$Nu = -\left[\frac{\partial\theta}{\partial y}\right]_{y=0} \tag{17}$$

The following is how we derive the Nusselt number from Eqs. (14) and (17).

$$Nu = \sqrt{H_1 Q}\,\mathrm{erf}\left(\sqrt{Q\,t}\right)+\sqrt{\frac{H_1}{\pi t}}e^{-Qt}$$

3.3 Sherwood Number

When y = 0, the Sherwood number is determined by

$$Sh = - \left[\frac{\partial \phi}{\partial y} \right]_{y=0} \tag{18}$$

The following is how we derive the Sherwood number using Eqs. (15) and (18). $Sh = \sqrt{Sc\ Kr}\,\mathrm{erf}\left(\sqrt{Kr\ t}\right) + \sqrt{\frac{Sc}{\pi t}} e^{-Kr\ t}$

Here

$$H_1 = \frac{\mathrm{Pr}}{1 + R},\ H_2 = \frac{1}{1 + \lambda},\ H_3 = \frac{1}{H_2},\ H_4 = M\sin^2\alpha + \frac{1}{K}.$$

4 Results and Discussion

In relation to this physical problem, graphs and tables have been used to discuss the frequency of velocity, the rate of heat transfer, temperature, the rate of mass transfer, and velocity by providing numerical ranges to the quantities M, K, t, λ, α, Pr, Sc, Kr, $Q > 0$, *and* w. The results of the comparison show sufficient agreement to support the validity of this numerical approach.

In Fig. 1, with an increase in the magnetic parameter M, it appears that the flow's velocity is greatly lowered. The Lorentz force, which attempts to impede the flow, was produced by the magnetic parameter M's rising value. As a result, the velocity curve flattens out as the magnetic parameter increases. The relationships between the values of (K) and (t) and the liquid velocity curve are shown in Figs. 2 and 3. The liquid velocity curve is seen to increase along with the fluid flow's (K) and (t) parameters. Figures 4 and 5 depict how the Jeffrey liquid quantity (λ) and oriented angle (α) affect the fluid velocity. It is noticeable that as the fluid flow's Jeffrey liquid quantity (λ) and oriented angle (α) increase, the velocity decreases. The liquid velocity curve remained constant, as shown in Fig. 6, as the time interval quantity (w) in the fluid flow increased. Figures 7, 8, and 9 exhibit how various flow variables influence fluid temperature. The Prandtl number is stated as a function of kinematic viscosity and thermal diffusivity. The relationship between the liquid temperature and the Prandtl number (Pr) and heat emission quantity (Q > 0) is shown in Figs. 7 and 8. The temperature drops as the Prandtl number (Pr), or the quantity of the heat source (Q > 0), increases in the liquid flow. The relationship between amount (R) and liquid temperature appears in graph (Fig. 9). Figures 10 and 11 illustrate how the *Sc* number and chemical quantity (Kr) have an impact on the fluid concentration. The concentration was found to fall as the Sc number or the (Kr) increased.

The Nu, Sh, and skin-graft coefficients' shifts are shown in Table 1. As *M* or α grows, the skin-graft coefficient falls, and as λ, *K,* or *t* increases, the skin-graft
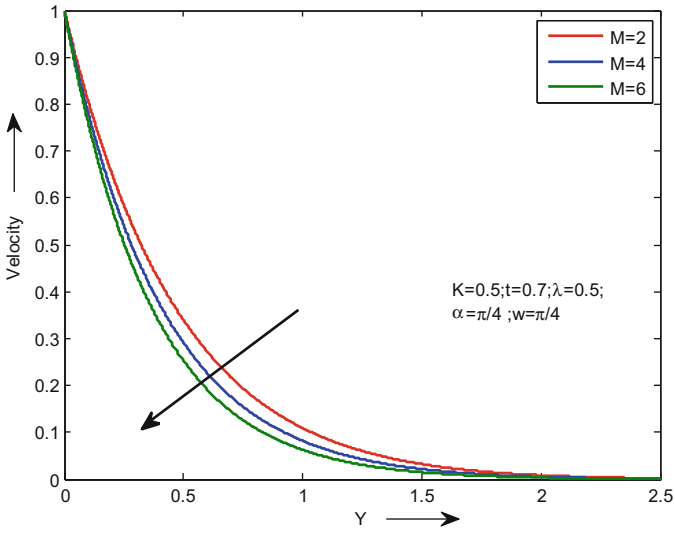
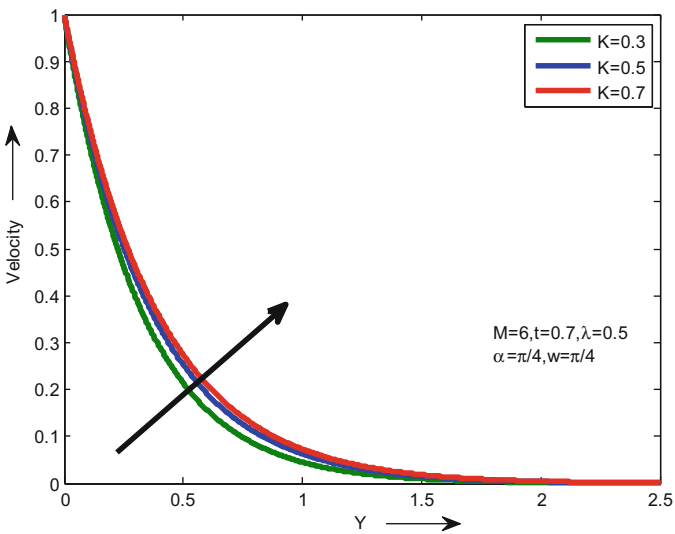**Fig. 1** Velocity lineation for variegated ranges of M

Fig. 2 Velocity lineation for variegated ranges of K

coefficient grows. As R rises, the Nu number falls, and as Pr or Q rises, the Nusselt number rises. As Sc or Kr rises, Sh number rises.
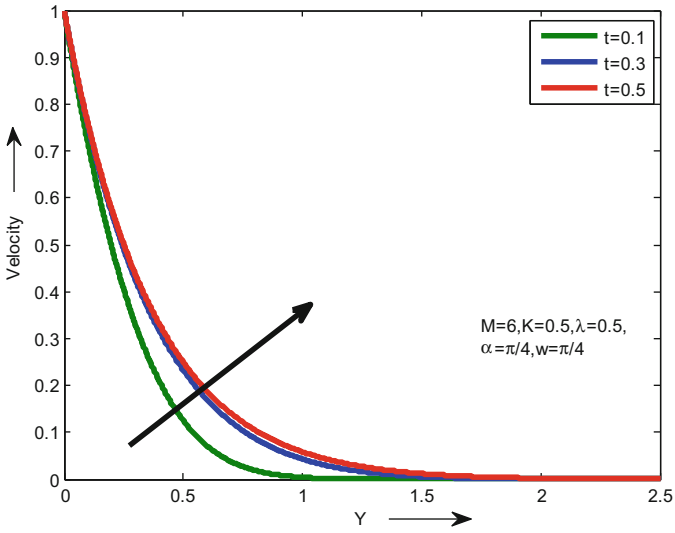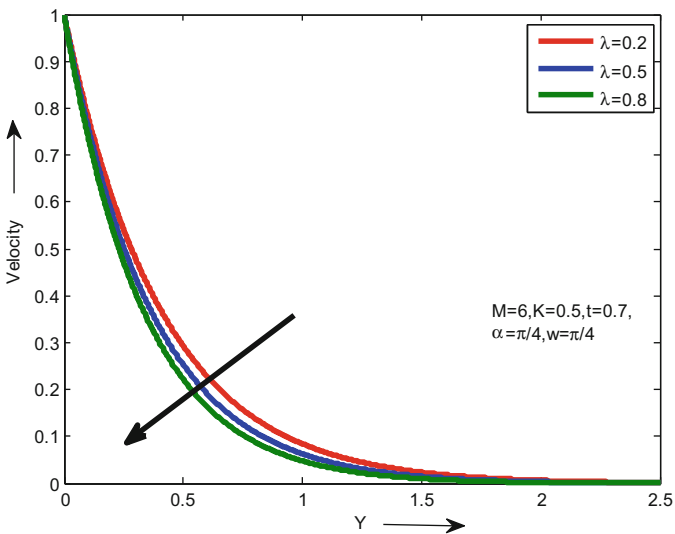
Fig. 3 Velocity lineation for variegated ranges of *t*

Fig. 4 Velocity lineation for variegated ranges of λ

5 Conclusion

In this work, consideration was given to the non-Newtonian Jeffrey fluid's steady flow, which is necessary for heat and mass transmission in porous media. The emerging parameters' effects are listed.
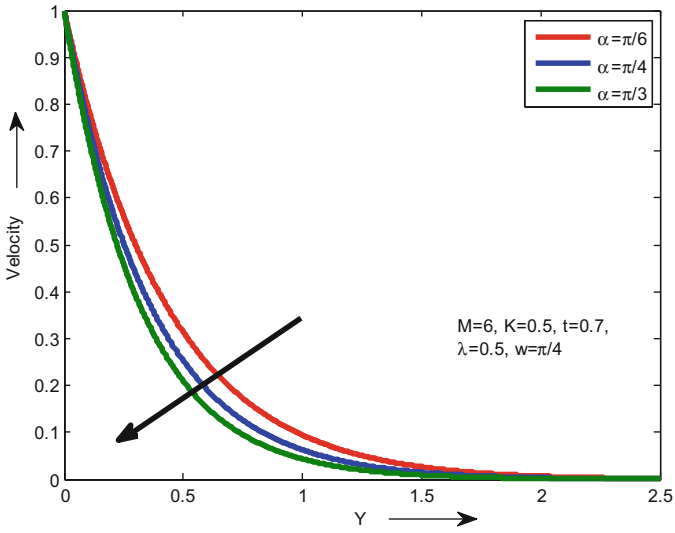
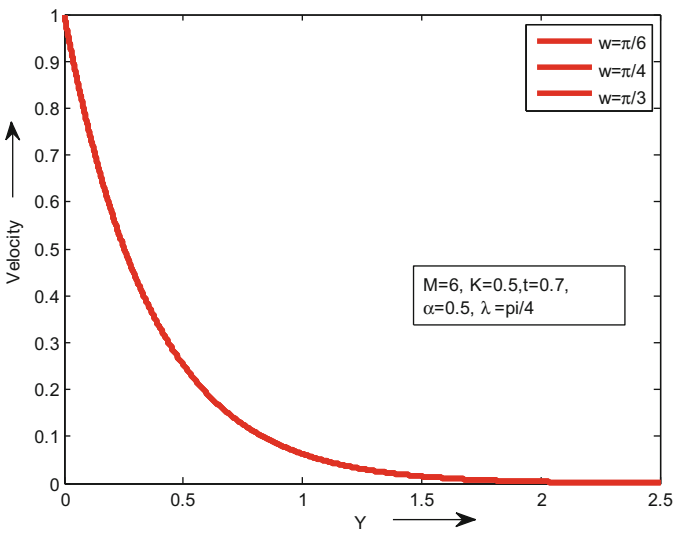**Fig. 5** Velocity lineation for variegated ranges of α

Fig. 6 Velocity lineation for variegated ranges of w

1. The process of heat and mass transport is significantly impacted by the magnetic amount (M).
2. Reduced heat- and mass-transfer rates are caused by increases in M, λ, α, Pr, or Q.
3. The heat and mass transfer, however, increase as K, t, R, Sc, or Kr grows.
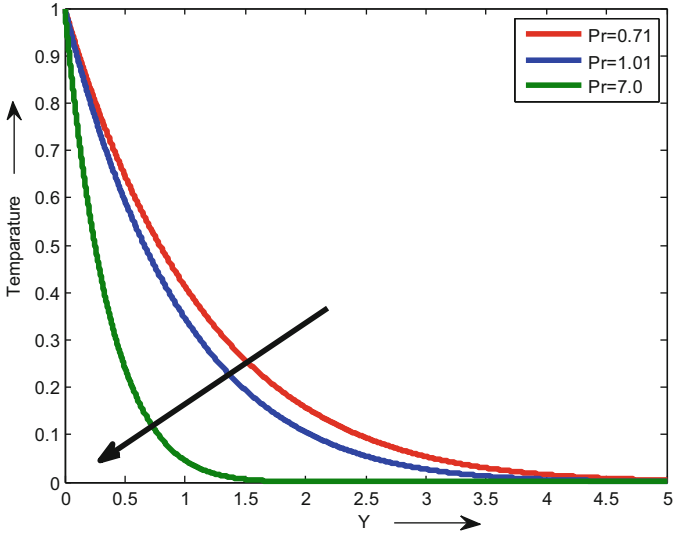
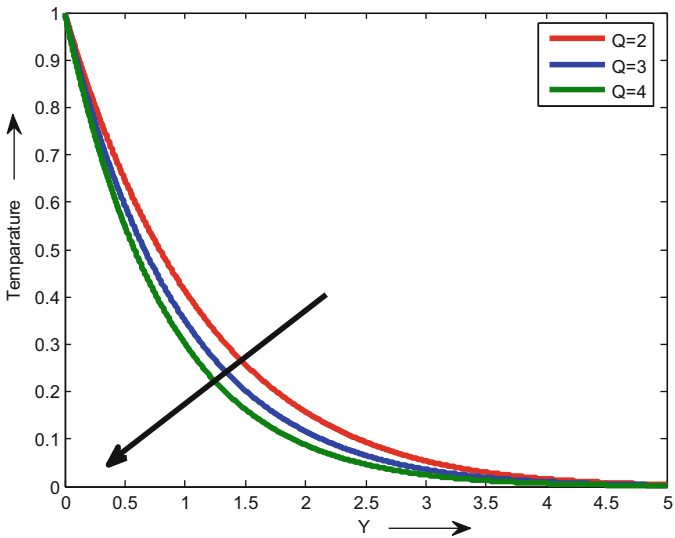**Fig. 7** Temperature lineation for variegated ranges of *Pr*

Fig. 8 Temperature lineation for variegated ranges of *Q*

4. The amount of skin graft decreases as the Jeffrey fluid flows, yet mass and heat transmission efficiency at the surface is found to slightly rise.
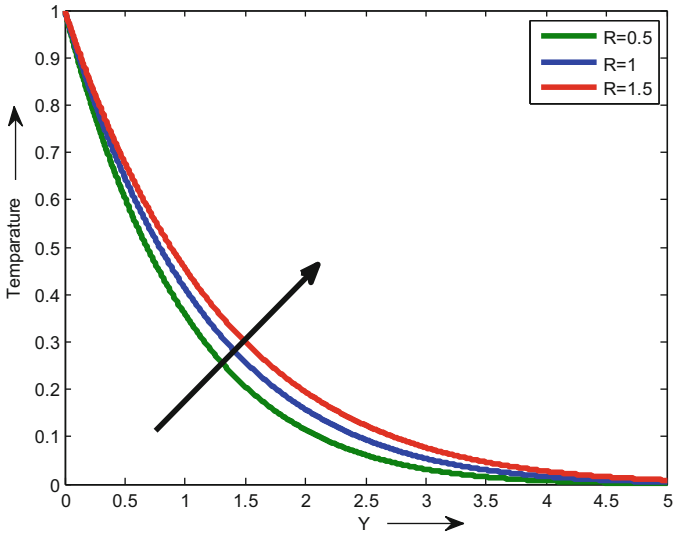
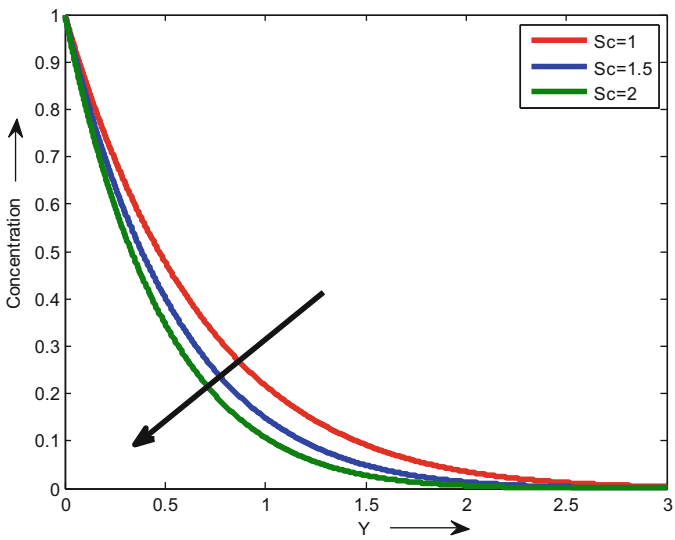**Fig. 9** Temperature lineation for variegated ranges of *R*

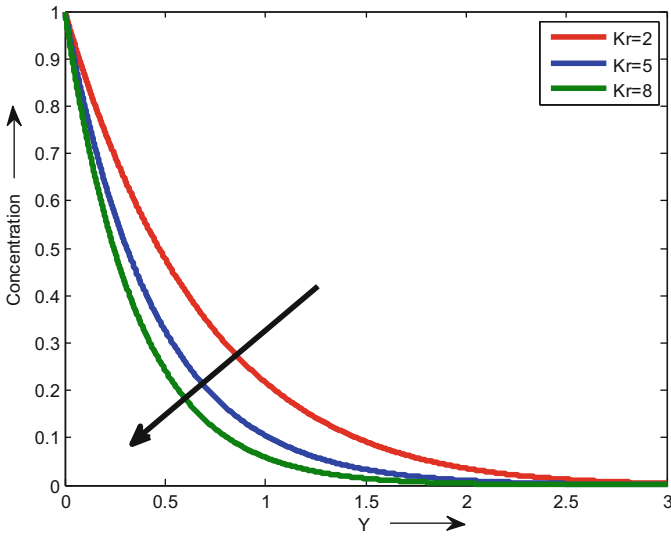

Fig. 10 Concentration lineation for variegated ranges of *Sc*

Fig. 11 Concentration lineation for variegated ranges of *K*

Table 1 Skin-friction coefficient, Nusselt number, and Sherwood number

M	λ	t	w	K	A	Pr	Q	R	Kr	Sc	τ	Nu	Sh
2	0.5	1	π/4	0.5	π/4	0.71	2	1	0.5	0.22	−1.4169	0.8498	0.3869
3											−1.5290		
4											−1.6338		
	0.6										−1.3719		
	0.7										−1.3310		
		2									−1.4297		
		3									−1.4274		
			π/6								−1.4169		
			π/3								−1.4169		
				0.6							−1.3374		
				0.7							−1.2780		
					π/6						−1.2961		
					π/3						−1.5290		
						1.01						1.0135	
						7						2.6682	
							3					1.0340	
							4					1.1922	
								2				0.6938	
								3				0.6009	
									0.7				0.4309
									0.9				0.4726
										0.62			0.6496
										0.96			0.8083

References

1. Rundora, L., Makinde, O.D.: Analysis of unsteady MHD reactive flow of non-Newtonian fluid through a porous saturated medium with asymmetric boundary conditions. Iran. J. Sci. Technol. Trans. Mech. Eng. **40**(3), 189–201 (2016)
2. Reddy, J.V., Sugunamma, V., Sandeep, N.: Effect of aligned magnetic field on Casson fluid flow past a vertical oscillating plate in porous medium. J. Adv. Phys. **5**(4), 295–301 (2016)
3. Jena, S., Mishra, S.R., Dash, G.: Chemical reaction effect on MHD Jeffery fluid flow over a stretching sheet through porous media with heat generation/absorption. Int. J. Appl. Comput. Math. **3**(2), 1225–1238 (2017)
4. Sailaja, M., Reddy, R.H., Saravana, R., Avinash, K.: Aligned magnetic field effect on unsteady liquid film flow of Casson fluid over a stretching surface. In: IOP Conference Series: Materials Science and Engineering, vol. 263, No. 6, p. 062008. IOP Publishing (2017). https://dx.doi.org/10.1088/1757-899X/263/6/062008
5. Saranya, S., Al-Mdallal, Q.M.: Non-Newtonian ferrofluid flow over an unsteady contracting cylinder under the influence of aligned magnetic field. Case Stud. Therm. Eng. **21**, 100679 (2020)
6. Santoshi, P.N., Reddy, G.V.R., Padma, P.: Flow features of non-Newtonian fluid through a parabolic of revolution. Int. J. Appl. Comput. Math. **6**(3), 1–22 (2020)
7. Kumar, C.P.: Thermal diffusion and inclined magnetic field effects on MHD free convection flow of Casson fluid past an inclined plate in conducting field. Turk. J. Comput. Math. Educ. **12**(13), 960–977 (2021)
8. Rama Prasad, J.L., Balamurugan, K.S., Varma, S.V.K.: Aligned magnetic field effect on unsteady MHD double diffusive free convection flow of Kuvshinski fluid past an inclined moving porous plate. In: Advances in Fluid Dynamics, pp. 255–262. Springer, Singapore (2021)
9. Endalew, M.F., Sarkar, S.: Incidences of aligned magnetic field on unsteady MHD flow past a parabolic accelerated inclined plate in a porous medium. Heat Tran. **50**(6), 5865–5884 (2021)
10. Abd-Alla, A.M., Abo-Dahab, S.M., Thabet, E.N., Abdelhafez, M.A.: Impact of inclined magnetic field on peristaltic flow of blood fluid in an inclined asymmetric channel in the presence of heat and mass transfer. Waves Random Complex Media, **32**, 1–25 (2022)
11. Kodi, R., Konduru, V.: Heat and mass transfer on MHD convective unsteady flow of a Jeffrey fluid past an inclined vertical porous plate with thermal diffusion Soret and aligned magnetic field. Mater. Today Proc. **50**, 2128–2134 (2022)
12. Nazir, S., Kashif, M., Zeeshan, A., Alsulami, H., Ghamkhar, M.: A study of heat and mass transfer of non-Newtonian fluid with surface chemical reaction. J. Indian Chem. Soc. **99**(5), 100434 (2022)
13. Arshad, M., Hussain, A., Hassan, A., Shah, S.A.G.A., Elkotb, M.A., Gouadria, S., Galal, A.M.: Heat and mass transfer analysis above an unsteady infinite porous surface with chemical reaction. Case Stud. Therm. Eng. **36**, 102140 (2022)